Ultrafast Dynamics of Transition Metal Carbonyls: Photodissociation of $Cr(CO)_6$ and $Cr(CO)_6 \cdot (CH_3OH)_n$ Heteroclusters at 280 nm

Michael Gutmann,*,† Jörg M. Janello, Markus S. Dickebohm, Markus Grossekathöfer, and Jürgen Lindener-Roenneke

Institut für Physikalische Chemie, Luxemburger Strasse 116, D-50939 Köln, Germany

Received: November 24, 1997; In Final Form: February 6, 1998

We report on first results of real-time studies on the photodissociation dynamics of electronically excited $Cr(CO)_6$ and $Cr(CO)_6 \cdot (CH_3OH)_n$ heteroclusters generated in a molecular beam. The red part of the $^1T_{1u}$ metal to ligand charge-transfer state at 280 nm is excited, and the resulting photofragments are detected by multiphoton ionization. The decarbonylation dynamics is found to be much faster than the cross correlation width (230 fs) of our pump and probe pulses. The observed fragmentation pattern and its dynamics can tentatively be attributed to two competing dissociation channels, both starting from the primary photofragment $Cr(CO)_5$, a simultaneous and a sequential channel. For the clusters we find that both these channels appear to be operative depending on pump laser intensity and that decarbonylation precedes evaporative loss of solvent molecules, which takes place on the picosecond time scale. Solvated cluster species as well as coordinatively unsaturated carbonyls are stabilized by evaporation.

1. Introduction

Transition metal carbonyls are model systems for organometallic compounds, which are important for, for example, producing metal films by vapor deposition[1] and catalysis of olefin isomerization and oligomerization.[2] Particularly the metastable coordinatively unsaturated species are of relevance in this respect. Therefore the spectroscopy and dynamics of coordinatively unsaturated transition metal carbonyls have received considerable attention throughout the literature, and a large number of experimental studies on the group VIb hexacarbonyls $Cr(CO)_6$, $Mo(CO)_6$, and $W(CO)_6$ and on $Fe(CO)_5$ in condensed phase and in gas phase have been performed during the last two decades. As quite a large body of important results on the photofragmentation of those systems has been accumulated, it appears to be in order to summarize some of the work relevant to our study.

Condensed-Phase Studies. From IR spectroscopy after UV excitation of group VIb hexacarbonyls ML_6 (M = metal, L = CO) in inert gas matrixes and by using isotopic labeling, the metastable coordinatively unsaturated photofragments ML_5, ML_4, and ML_3 could be characterized and their most stable structures were deduced to be a square pyramid (C_{4v}) for ML_5, octahedral cis-divacant (C_{2v}) for ML_4, and octahedral cis-trivacant (C_{3v}) for ML_3.[3−9] By investigating the matrix photochemistry of the primary photofragment ML_5 with polarized light, dichroic photodepletion caused by reorientation of ML_5 was observed.[8,9] These findings were explained by first formation of naked ML_5 in an excited electronic ^1E state (square pyramid, C_{4v}) after UV irradiation of the parent molecule ML_6, followed by second reorientation via a trigonal bipyramid D_{3h} structure (equilibrium structure of the initially formed ^1E state), and third return to a rotated square pyramid C_{4v} structure in the $^1A_1$ electronic ground state. Thus, mixing of the $^1A_1$ ground state and the ^1E excited state potential surfaces at the D_{3h} structure leading to internal conversion had to be invoked. From these matrix studies and earlier flash photolysis experiments[10,11] it was concluded that the primary coordinatively unsaturated photofragment following UV excitation in condensed phase is ML_5, formed by ejection of a single CO ligand. After formation the naked ML_5 photofragment coordinates a solvent molecule or atom (S) or reformation of the parent via cage recombination occurs.[12] Further absorption of photons by ML_5 can lead to the higher coordinatively unsaturated species down to ML_2[5] (sequential model).

This interpretation has been confirmed after a series of time-resolved studies on the femtosecond (fs) and the picosecond (ps) timescale.[12−23] Simon and co-workers observed in their transient absorption measurements in the visible after UV photolysis of CrL_6 in hexane a pulse width limited (<1 ps) rise of CrL_5.[13−15] In methanol solution they observed a rise time of 2.5 ps, which they assigned to formation of CrL_5S. Spears and co-workers established a kinetic scheme containing two channels for formation of the complexed CrL_5S species, one channel via a square pyramidic structure and the other via a trigonal bipyramidic structure, the latter being the faster one.[16,17] Harris and co-workers found that the solvation dynamics of CrL_5 is controlled by vibrational cooling.[18] Joly and Nelson used fs pulses (308 nm pump pulse, visible probe pulse) for transient absorption measurements after photolyzing ML_6 in various alcohols and hexane with a time resolution of 100 fs.[19,20] They concluded that the primary step, i.e., ejection of the first CO ligand from ML_6, is completed within 350 fs; coordination of naked ML_5 with methanol to form ML_5S occurs within 1.6 ps, in agreement with the results of the Simon group.[14] Vibrational relaxation of ML_5S was estimated to take place on the order of 50 ps, depending on the specific solvent used. Harris and co-workers reported on dual cooling rates of ML_5S from visible transient absorption experiments.[21] A slow cooling time for CrL_5S in cyclohexane of about 150 ps was observed, which was assigned to relaxation of the high-frequency CO stretching vibrations to lower frequency molecular modes due to weak vibrational coupling. Dougherty and Heilweil using transient

† e-mail: gutmann@fock.pc.uni-koeln.de.

S1089-5639(98)00308-9 CCC: $15.00
Published on Web 04/09/1998

IR spectroscopy found for all ML_5S species a vibrational relaxation time for the excited CO stretching mode of 150 ps.[22] A recent fs-study on ML_6 in alkane solutions with UV photolysis pulses and IR transient absorption (240 fs cross correlation width) by Harris and co-workers was aimed at the short time dynamics of these species.[23] The authors interpreted the observed bleach recovery results in terms of fast geminate recombination within about 150 fs. After pulse width limited production of ML_5 fast reformation of the vibrationally hot ground-state parent molecule competes with formation of ML_5S, which vibrationally relaxes on the ps time scale.

Gas-Phase Studies. In the gas phase, decarbonylation of transition metal carbonyls is dominated by wavelength-dependent multiple ligand loss, which is in contrast to the condensed-phase behavior. Furthermore, we have to distinguish between single-photon and multiphoton pathways. Single-photon absorption with multiple ligand loss in the gas phase can occur since the amount of excess energy deposited in the parent molecule after UV excitation is sufficient to lead to dissociation of several ligands, whereas in condensed phase excess energy can efficiently be dissipated by the surrounding bath molecules. Further fragmentation of the photofragments can be explained by additional photon absorption of the primary photoproducts (sequential mechanism). Chemical trapping studies revealed the primary metastable coordinatively unsaturated photofragments in the single-photon case.[24−26] Exciting CrL_6 at 248 nm, Yardley and co-workers detected CrL_4, CrL_3, and CrL_2 fragments, with CrL_4 dominating the yield (73%). Additional studies confirmed CrL_4 to be the major photoproduct.[27,28] Photolyzing at 351 nm yielded CrL_5 as the main photofragment.[27,29] The same result was observed for M = W.[30] At higher laser fluences secondary photofragmentation of CrL_4 becomes important, yielding predominantly CrL_2.[28] Weitz and co-workers applied transient IR spectroscopy after UV excitation (248 nm) of gaseous ML_6 and confirmed the structure of the photofragments found in the matrix work (vide supra).[31−34]

Mikami, Ohki, and Kido studied the photodissociation of CrL_6 seeded in a molecular beam by two-color multiphoton dissociation/multiphoton ionization (MPD/MPI) and observed coordinatively unsaturated photofragments in the mass spectrum with the bare metal ion dominating.[35] The results were interpreted in terms of the sequential dissociation mechanism. Vernon and collaborators studied the MPD mechanism of group VIb hexacarbonyls (M = Cr, Mo, W) seeded in a molecular beam at 248 nm by measuring photofragment velocity distributions after electron impact ionization of the neutral products.[36] They proposed a mechanism where ML_6 after absorption of one photon loses a single CO ligand very rapidly (nonstatistical process) to form electronically excited ML_5 (C_{4v}) after converting to the vibrationally excited ground state (C_{4v}) via D_{3h} geometry to yield ML_4 (C_{2v}) thermally. Peifer, Garvey, and DeLeon investigated the photofragmentation of CrL_6 seeded in a molecular beam[37] by ns pump/probe spectroscopy and interpreted their results by sequential MPD via an intermediate CrL_4, in agreement with the mechanism proposed by Vernon and collaborators.[36]

Quite recently, Qi et al. measured absolute single-photon cross sections for photoabsorption, photodissociation, and photoionization of group VIb transition metal carbonyls above the first ionization potential using synchrotron radiation in the VUV range.[38] Similar to the UV range of interest here, they found fast neutral photodissociation competing favorably with autoionization. The same groups measured appearance potentials of the photofragments and obtained bond dissociation energies of CrL_6 and MoL_6 in the ionic manifold.[39,40]

With MPI of transition metal carbonyls in a molecular beam at 280 nm Duncan, Dietz, and Smalley found that the bare metal ion dominated the mass spectra of FeL_5, CrL_6, and MoL_6 by far.[41] Higher fragments could only be observed at very low laser intensities. From UV MPI spectra of FeL_5 Whetten, Fu, and Grant obtained upper bounds for the lifetimes of electronic excited states of less than 2 ps (300−310 nm) and less than 600 fs (270−280 nm).[42] Vaida and co-workers studied UV/visible MPD of CrL_6 monitoring emission from electronically excited Cr atoms.[43] They found strongly flux dependent thermal distributions, indicating different competing pathways to fragmentation. Increasing the photon flux could lead to multiphoton absorption giving preference to higher photon dissociation channels. Tyndall and Jackson studied MPD of CrL_6 at various UV excimer laser wavelengths.[44−47] They collected emission from electronically excited photofragments[44,45] and found a statistical distribution of the excited electronic states observed. From the quenching behavior a mechanism was deduced where the parent molecule absorbs a number (at least two) of photons coherently, ending up in a highly excited state. From that state explosive dissociation of all ligands promoted by multiple potential surface crossings in the outgoing channels could take place, leaving electronically excited Cr atoms behind.

Up to now two real-time studies with fs lasers focusing on the photodynamics of transition metal carbonyls in the gas phase have appeared in the literature. In a pioneering study by Zewail and co-workers the competition between metal−metal and metal−ligand bond breakage in Mn_2L_{10} seeded in a molecular beam was investigated.[48] It was found that the Mn−L bond breaks faster (∼20 fs) than the Mn−Mn bond (∼40 fs). Gerber and co-workers studied the photodissociation dynamics of FeL_5 expanded into vacuum.[49] They used the second harmonic of their Ti:Sapphire laser system for multiphoton photolysis and the fundamental output (pulse duration: 80 fs) for MPI. Transients of all occurring photofragments were measured. The parent molecule was found to decay faster than the laser pulse width, which they interpreted by dissociation from the optically accessed state to electronically excited fragment states. Due to the similar decay times of $FeL_{n=2-5}$, the following model was proposed: After excitation to an electronic state at 50 000 cm^{-1} the parent rearranges structurally during 20 fs (probe photons lead to parent ions, which fragment to FeL_4^+), obtains a different configuration after 30 fs (probe photons lead to parent ions, which fragment to FeL_3^+), and undergoes an additional change of structure, which analogously yields FeL_2^+. The observed decay times of 100 fs could thus be explained by the parent losing four ligands as the rise time of FeL was measured to be 120 fs. FeL decayed to a constant level within 230 fs, close to the Fe rise time of 260 fs.

To bridge the gap between condensed phase and gas phase and elucidate the different mechanisms of transition metal carbonyl photofragmentation in both phases, Peifer and Garvey investigated $CrL_6 \cdot S_n$ and $FeL_5 \cdot S_n$ (S = CH_3OH) van der Waals heteroclusters produced in a molecular beam.[50−52] For $CrL_6 \cdot S_n$ fragment analysis after MPI at 248 nm with moderate laser intensities of 2×10^7 W/cm^2 showed a number of solvated coordinatively unsaturated photofragment ions.[50] Comparing with high-fluence experiments ($10^{12}-10^{13}$ W/cm^2)[51] at 248 nm and around 350 nm the authors could rule out a MPI/MPD mechanism and in contrast to condensed-phase studies found a wavelength-dependent fragmentation pattern, which they attributed to the specific electronic state of CrL_6 excited primarily.

At 248 nm solvated CrL_4 and at 350 nm solvated CrL_5 were proposed to be the primary neutral photofragments in order to explain the observed wavelength-dependent fragmentation pattern.

Theoretical Studies. In addition to the experimental work, a number of theoretical studies concerning the electronic structure and spectra of transition metal carbonyls have been performed.[53−59] In a pioneering study Beach and Gray investigated the electronic spectra of group VIb transition metal carbonyls in the gas phase and in solution. They based their assignments on semiempirical molecular orbital (MO) calculations.[53] Hay studied the electronic structure of the photofragment CrL_5 by means of ab initio calculations with configuration interaction (CI) using a small Gaussian basis set.[54] He confirmed the experimental findings that the C_{4v} (square pyramid) $^1A_1$ state is the energetically lowest lying electronic state of CrL_5. The visible excitation at 500 nm was assigned to the $^1E \leftarrow {}^1A_1$ transition (C_{4v}). With CASSCF/CASPT2 calculations Pierloot, Roos, and collaborators investigated the electronic ground state as well as excited states of CrL_6.[57,58] From their calculations the previous assignments of the electronic spectra[53] had to be reconsidered. Particularly, the ligand field (LF) states were calculated to be at much higher energies than had been assigned before. Thus photofragmentation at 350 nm may have to be reinterpreted in terms of MLCT states. Baerends and co-workers confirmed these results by density functional calculations.[59] The low lying electronically excited states were assigned to symmetry-forbidden charge-transfer transitions. Potential curves along the Cr−CO coordinate were calculated to be repulsive, leading to photodissociation from charge-transfer states. The high lying LF states were calculated to be highly dissociative along the metal to ligand bond and may cross lower lying states during dissociation.

In this contribution we shall report on our first results on the fs dynamics of CrL_6 in the gas phase and of $CrL_6 \cdot S_n$ ($S = CH_3OH$) heteroclusters. The aim of this ongoing research is to contribute to an understanding of the reaction dynamics of transition metal carbonyls both in the gas phase and in condensed phase by systematically studying their solvent clusters. It is hoped that the different dynamics in both regimes can be understood by means of investigating the cluster dynamics.

In section 2 the experimental setup will be described; in section 3 we shall present our results and discuss them referring to models that have been proposed in the literature. The contribution will be concluded by some final remarks in section 4.

2. Experimental Section

The laser system schematically shown in Figure 1 is based on a femtosecond Ti:Sapphire amplifier (BMI, Alpha 10 series), which amplifies pulses of an argon ion laser (Coherent, Innova 310) pumped Ti:Sapphire oscillator (Coherent, Mira Basic) at a 10 Hz repetition rate. The amplifier consists of a reflective stretcher, a Nd:YAG laser (532 nm) pumped regenerative amplifier, a four-pass bowtie amplifier pumped by the same Nd:YAG laser (532 nm), and a two-grating compressor. The output pulses centered at 805 nm have about 17 mJ of energy and a pulse duration of 80−100 fs, as is routinely verified by single-shot autocorrelation. The time bandwidth product translates to approximately 1.5 times the transform limit assuming a $sech^2$ functional intensity autocorrelation shape. These fundamental pulses of about 12 mm diameter are frequency doubled in a 0.5 mm thick BBO I crystal yielding pulses of up

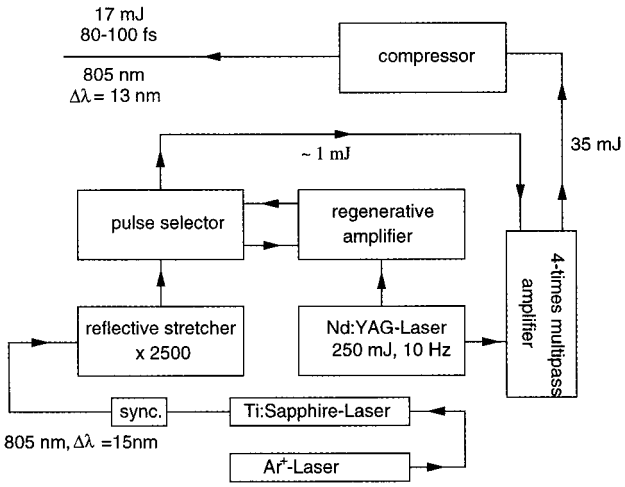

Figure 1. Schematic sketch of the fs laser system.

to 7 mJ centered at 402.5 nm. The remaining fundamental after appropriate attenuation is used to generate a white light continuum providing seed pulses for two home-built optical parametric amplifiers (OPAs, Figure 2). The OPAs are simultaneously pumped by the 402.5 nm fs pulses. The OPA design is based on a setup published by Greenfield and Wasiliewski[60] and consists of a BBO II white light preamplifier, a BBO I main amplifier, and a double-pass two-prism (SF 10) compressor. Typical output pulses in the visible have energies of up to 100 μJ and a pulse duration of less than 150 fs. For the one-color pump/probe experiments discussed here, we tuned both OPAs to a center wavelength of 560 nm. The output of one OPA was delayed with respect to the other via the usual Michelson interferometer type setup. The delay stage (Aerotech, ATS 0230 with stepper motor) has a resolution of 0.1 μm. Both OPA pulses are combined on a beamsplitter and sent into a 0.2 mm thick BBO I doubling crystal in order to obtain fs pulses centered at 280 nm. The cross correlation between the two 560 nm pulses was measured routinely and yielded a typical width (full width at half-maximum, fwhm) of 230 fs (Figure 3), which is not expected to change after frequency doubling in the 0.2 mm BBO I crystal. The femtosecond UV pulses are then focused into the molecular beam.

The molecular beam apparatus (Figure 4) consists of two differentially pumped chambers, a main chamber pumped by a 400 l/s turbomolecular pump (Leybold) backed by a two stage roughing pump (Edwards, E2M18) and a buffer chamber pumped by a 300 l/s turbomolecular pump (Edwards, EXT 351) backed by a second two-stage roughing pump (Edwards, E2M8). Both chambers are separated by a rhodium-plated nickel skimmer (Beam Dynamics) of 1.5 mm diameter. The main chamber contains the nozzle assembly, which can be translated via a rotatory feedthrough. The pulsed solenoid molecular beam valve (General Valve, Series 9) with a home-built conical orifice of 0.2 mm diameter is connected to a sample holder and the buffer gas inlet. Both the nozzle and the sample compartment can be heated. The nozzle is driven by a home-built triggering and driver assembly and delivers clean gas pulses of about 100 μs duration, which are regularly checked by electron impact ionization. The buffer chamber houses a home-built time-of-flight (TOF) mass spectrometer whose flight tube is pumped by a 200 l/s turbomolecular pump (Edwards, EXT 200) backed by the second roughing pump. The TOF mass spectrometer is of Wiley-McLaren type[61] and includes an Einzel lens assembly to focus the ions onto a two-stage microchannel plate (Hamamat-

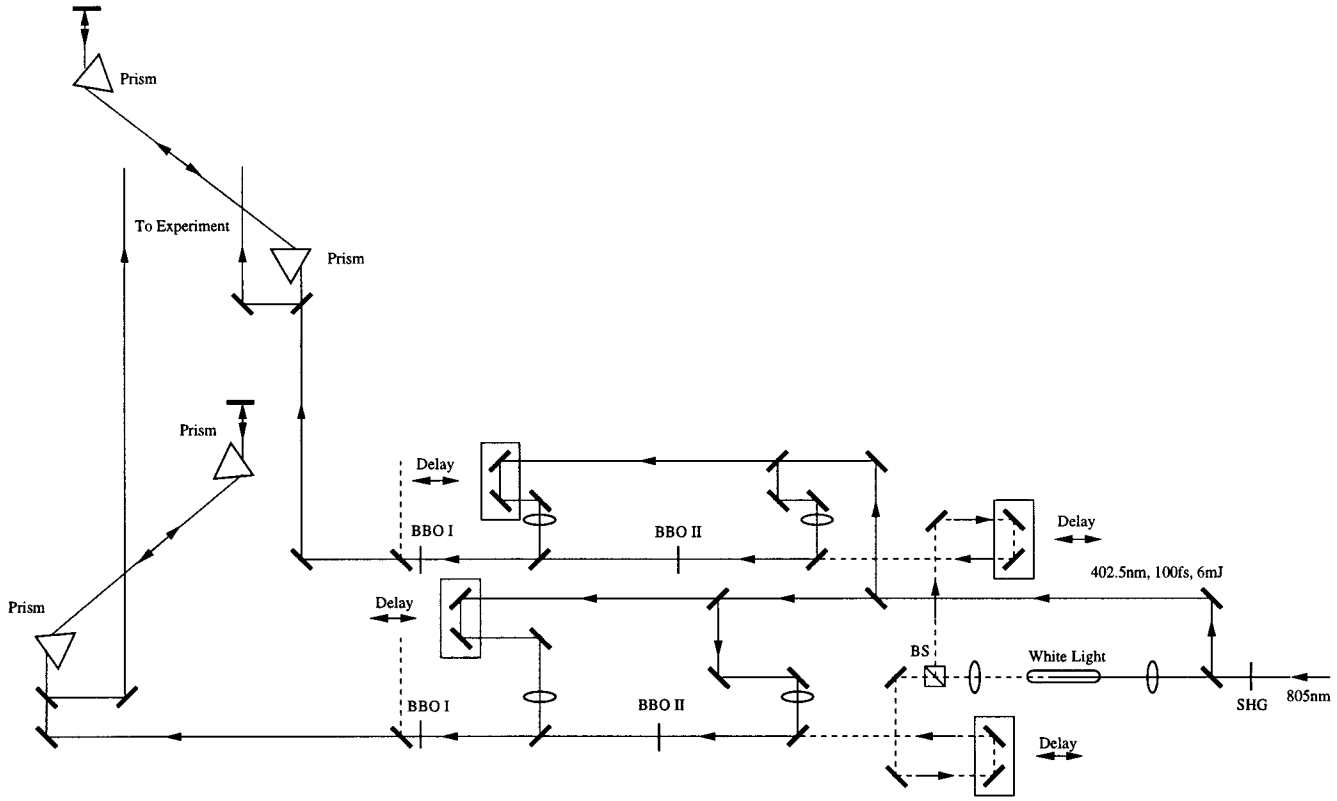

Figure 2. Outline of the two simultaneously pumped white-light-seeded double-stage optical parametric amplifiers with prism compressors.

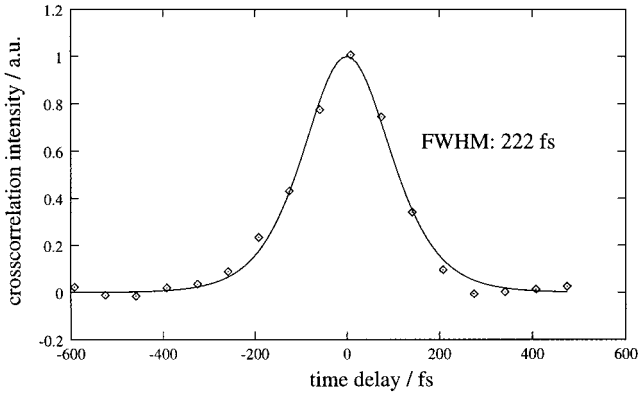

Figure 3. Typical intensity cross correlation of the pump and probe pulses prior to SHG (fwhm(sech^2) = 222 fs).

su, F1552-29S). For monitoring purposes and trigger adjustment, electron impact ionization is possible.

The experiments on pure $Cr(CO)_6$ were performed by expanding a heated (ca. 375 K) sample of $Cr(CO)_6$ (Aldrich, 99%, used as received) through the pulsed valve into vacuum. The $Cr(CO)_6{\cdot}(CH_3OH)_n$ heteroclusters were produced by bubbling Ne gas (Linde, 99.995%) through a reservoir of methanol (Merck, 99.8%) and seeding the beam at a backing pressure of ca. 3 bar with heated (ca. 375 K) $Cr(CO)_6$. The nozzle to skimmer distance was set to $x/d \sim 100$. The nozzle and the laser system were triggered externally at 10 Hz and synchronized such that laser pulses and gas pulses temporally overlapped in a region where cluster formation could be observed. With the nozzle on, the pressure in the main chamber was about 1.2×10^{-4} mbar and the pressure in the flight tube was less than 1.0×10^{-6} mbar.

The laser pulses had an incidence angle of 90° with respect to the gas pulses. The first laser pulse excited the red part of a $^1T_{1u}$ MLCT transition of $Cr(CO)_6$, from which the fragmentation dynamics started and the delayed probe laser ionized the nascent fragments. The ions were accelerated at an angle of 90° with respect to both the molecular beam and the laser beam by electrostatic deflection and extraction plates and detected by the multichannel plate whose signal output was amplified by a home-built amplifier and fed into a digital signal analyzer (Tektronix, DSA 601), where the resulting mass spectra were averaged for a preset number of shots (typically about 100 shots). The averaged mass spectra and the actual position of the delay stage were stored and sent to a microcomputer after each scan. The average laser intensity was monitored by a photodiode, which also triggered the DSA 601 to check any irregularity in signal strength. A number of scans (4−10) was averaged, and the transients for each mass peak of interest were generated from integrating the corresponding peak areas for each delay position. Data analysis was performed on a DEC Alpha workstation.

3. Results and Discussion

3.1. Dynamics of $Cr(CO)_6$. Figure 5 shows a mass spectrum of an expansion of pure $Cr(CO)_6$ obtained with fs pulses centered at 280 nm. From the figure it is apparent that the mass spectrum of pure $Cr(CO)_6$ is dominated by the bare metal ion signal, followed in intensity by $CrCO^+$, $Cr(CO)_2^+$, the parent ion $Cr(CO)_6^+$, and $Cr(CO)_3^+$. The signal of $Cr(CO)_4^+$ is very small, and $Cr(CO)_5^+$ is almost not present in the spectrum. It should be noted that the fs mass spectrum taken under MPI conditions differs considerably from the ns MPI spectrum, where only the bare metal ion is observed (see, for example reference 41). The appearance of the coordinatively less unsaturated carbonyls can be explained by the ladder switch model introduced by Schlag and co-workers.[62] Direct ionization can compete with fast photofragmentation of the neutral parent in the ultrafast regime, leading to parent and higher fragment ion signals. With ns lasers, however, fast photofragmentation

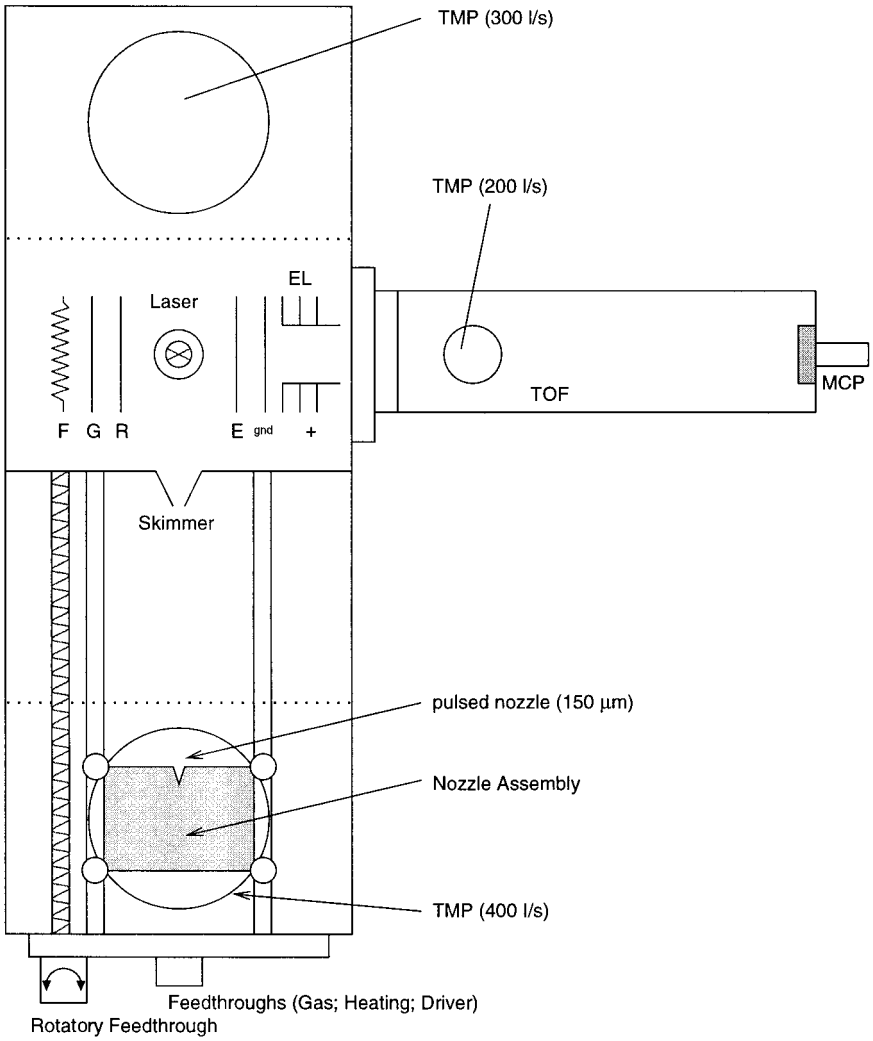

Figure 4. Molecular beam apparatus (F = filament, G = grid plate, R = repeller plate, E = extractor plate, EL = Einzel lens assembly, TMP = turbomolecular pump).

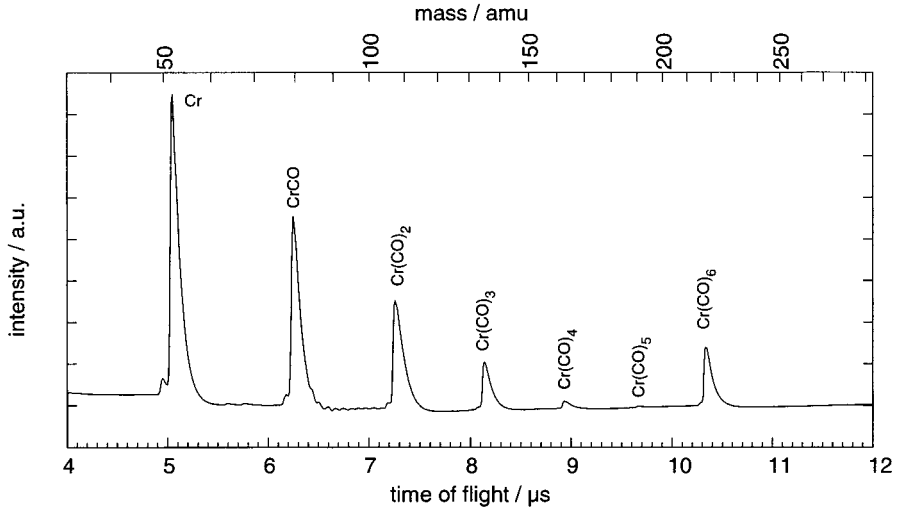

Figure 5. Averaged femtosecond mass spectrum obtained from an expansion of pure $Cr(CO)_6$.

in the neutral manifold will dominate, leading to ligand stripping and observation of only the bare metal ion. In the following we shall further argue that the strong fragmentation pattern is mainly due to fragmentation in the neutral manifold followed by ionization (absorption−dissociation−ionization, ADI scheme[63]) at the laser intensities applied here ($10^{10}-10^{11}$ W/cm^2), although we cannot yet rigorously prove this scheme. Applying much lower intensities, we obtained mass spectra that were dominated by the parent ion peak but also showed the fragments Cr^+, $CrCO^+$, and some $Cr(CO)_2{}^+$. The higher coordinated fragment ion peaks still could not be observed. These preliminary findings already indicate that fragmentation down to the bare metal if occurring in the neutral manifold must be extremely fast compared to our time resolution of <230 fs, as the higher

coordinated fragments are of very low signal strength. Multiphoton dynamics will be occurring rather than single-photon dynamics.

In the following we shall provide some arguments favoring interpretation of our results within the ADI scheme rather than the AID (absorption−ionization−dissociation) scheme.[63] The parent ion $Cr(CO)_6^+$ observed will most likely be generated by direct two-photon absorption of the ground-state molecule. According to the energetics (see Figure 6), absorption of two photons at 280 nm yields the parent ion in its electronic ground state with about 6100 cm^{-1} of excess energy. Part of this excess energy will be withdrawn as kinetic energy by the departing electron. Even the amount of 6100 cm^{-1} is not sufficient to break a Cr−CO bond in the parent ion. According to the results of Qi et al.,[39] at least 9600 cm^{-1} are needed. Thus, any fragment ions appearing in the mass spectrum must result either from neutral fragments or from ions that must have absorbed additional photons from the fs laser beam. The first electronically excited ion state lies about 6 eV above the ionic ground state,[64] which means that in order to arrive at that state at least three to four photons at 280 nm must be directly absorbed from the fs laser pulse. Although this possibility cannot be excluded when exciting with intense fs pulses, we think that it is more likely that the observed fragment ions arise from neutral species. Quite recently we became aware of fs work on the photofragmentation of pure $Cr(CO)_6$ carried out in the Kompa group by Trushin et al.[65] parallel to our studies. They pumped the $^1T_{1u}$ MLCT state using the third harmonic (267 nm) of their fs Ti:Sapphire laser system and probed by MPI with the fundamental (800 nm). They observed all photofragments including $Cr(CO)_4^+$ and $Cr(CO)_5^+$ at early times in the mass spectrum. By the energetics shown in Figure 6 these findings can be explained. With 267 nm pump wavelength ionization needs at least three photons at 800 nm, leading to a parent ion with 9700 cm^{-1} of excess energy, sufficient to break a Cr−CO bond to form $Cr(CO)_5^+$, which may thus arise from parent ionization. In the following we shall propose that the dynamics we observe is essentially due to extremely fast photofragmentation starting in the $^1T_{1u}$ MLCT state of the neutral parent. Ionic coordinatively unsaturated fragments must then be formed from ionized neutral photofragments, which means that photofragmentation in the neutral must occur during the pulse width of our laser (∼150 fs). Evidence for such fast photofragmentation in transition metal carbonyls has been provided recently by Gerber and co-workers for $Fe(CO)_5$.[49] Trushin et al., too, observed pulse width limited photofragmentation dynamics of $Cr(CO)_6$ in their experiments.

Figure 7 shows the transients obtained for $Cr(CO)_6^+$, $Cr(CO)_4^+$, $Cr(CO)_3^+$, and $Cr(CO)_2^+$, and Figure 8 shows those of $CrCO^+$ and Cr^+. As both pump and probe wavelength are identical, the transients are symmetric with respect to zero delay, T_0. Slight deviations from symmetry are caused by the fact that one of the beams was more intense than the other. On the right-hand side (positive delay time) the lower intensity beam is the pump beam, and on the left-hand side (negative delay) the higher intensity beam is the pump beam. For the parent down to $Cr(CO)_2^+$ pulse width limited transient peaks slightly separated from T_0 (about 150 fs) are observed, indicating very fast formation and decay of the corresponding neutral fragments. The initial rise of all transients is nearly instantaneous on the time scale of our pulses and could not be fitted when using a single-exponential rise convoluted with a Gaussian of our cross correlation width. A convoluted single-exponential with rise time of about 90 fs fits the slower part of the rising edge of the

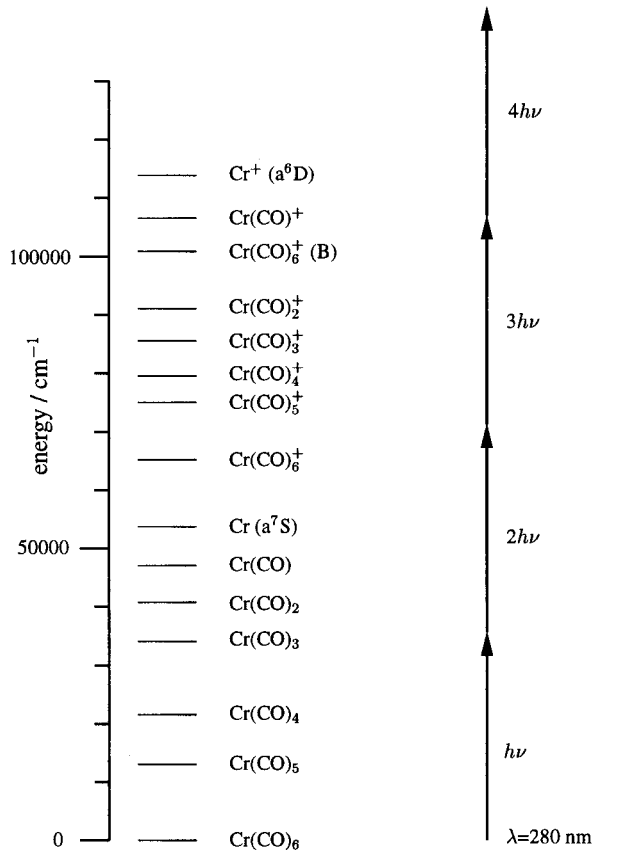

Figure 6. Energy diagram of $Cr(CO)_{n=0-6}$ in the neutral and the ionic manifold. Neutral first and second bond dissociation energies were taken from ref 66. The other neutral bond dissociation energies were calculated by dividing the remaining energy equally according to ref 50. The ionic data were taken from ref 39. The energetics of our laser pulses at 280 nm is shown as arrows.

Cr^+ transient rather well, and a similar fit for the $Cr(CO)^+$ transient yields 60 fs (see Figure 8b). It should be noted that these numbers have to be taken only as rough estimates since the cross correlation width of the laser pulses used in the experiments was 230 fs and the fits depend on the onset location for the slower part of the rise. In addition, the signal to noise ratio of our measurements has to be taken into account. However, we can at least confirm that the $Cr(CO)^+$ transient rises significantly faster than the Cr^+ transient. These observations may indicate that we possibly observe two types of dynamical processes, a quasi instantaneous one (dynamics A) and a second slower but still fast one (dynamics B). As will be shown when discussing the cluster experiments, dynamics A becomes more important as the pump laser intensity is increased. Thus we tentatively attribute dynamics A to multiphoton explosive loss of CO ligands as proposed by Tyndall and Jackson[44,45] and dynamics B to the initial stages of the common model for photofragmentation of $Cr(CO)_6$.[36] For $Cr(CO)_2^+$ and $Cr(CO)_3^+$ the transients decay down to a low nonzero level which is constant during the time delay (7.2 ps) covered, whereas the transients of $Cr(CO)_4^+$ and $Cr(CO)_6^+$ appear to decay down to zero. This may be taken as another point of evidence for existence of two different dynamical channels, as there are obviously two kinds of species for $Cr(CO)_2^+$ and $Cr(CO)_3^+$, a decaying species and a constant species in time. (It should be noted that the exact level of zero intensity cannot be easily determined at T_0 since due to the symmetry of the transients at negative delay and at positive delay with respect to T_0, there is some residual signal arising from

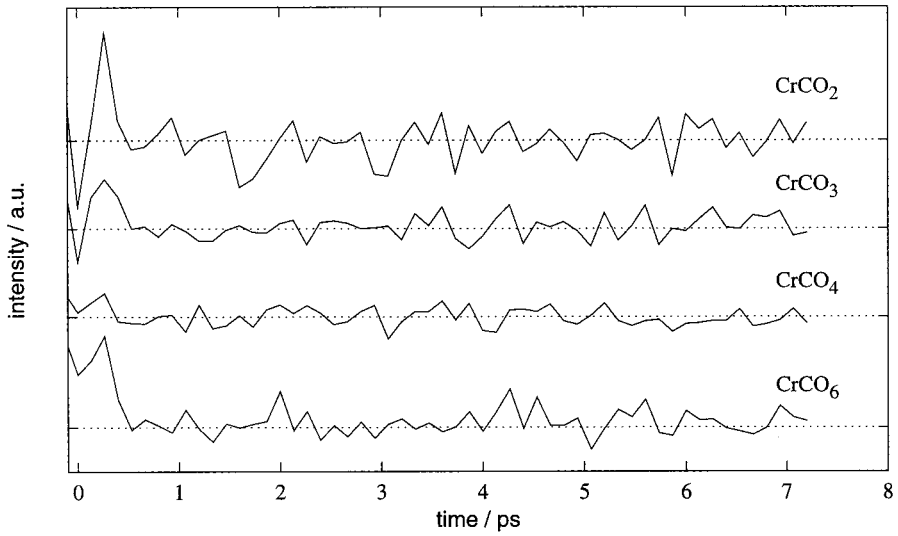

Figure 7. Transients of $Cr(CO)_{n=2,3,4,6}$ ions obtained from pure $Cr(CO)_6$. Dotted lines denote asymptotic averages on the time scale covered by the experiments. The transients are slightly offset with respect to each other.

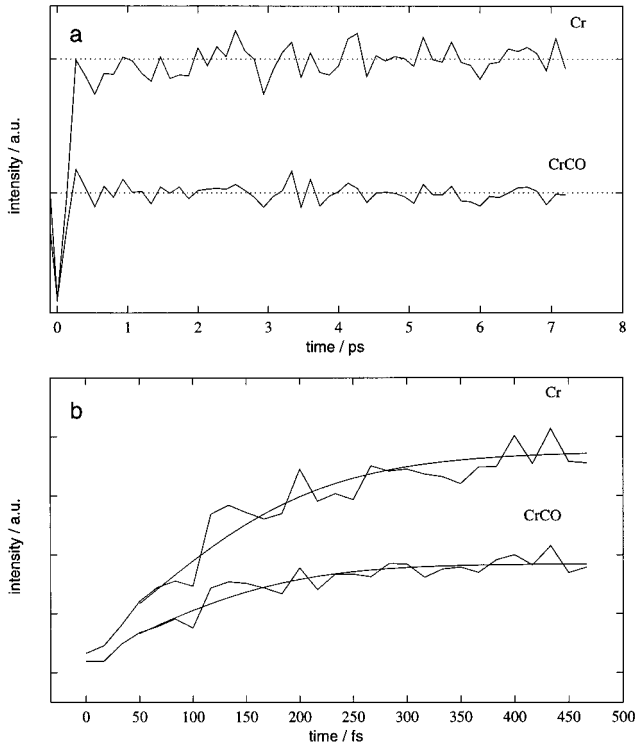

Figure 8. Transients of Cr and CrCO ions obtained from pure $Cr(CO)_6$. The rise at negative time delay is due to the symmetry inherent in the one-color pump/probe scheme used here. (a) Transients obtained on a longer time scale (step size: 133 fs). (b) Transients obtained at short delay times (step size: 16.7 fs). Shown are fits to a single-exponential rise convoluted with a Gaussian of experimental cross correlation width. The rise times are $\tau_{Cr} = 87$ fs, $\tau_{CrCO} = 63$ fs.

the overlap of both transients around T_0, whose level depends on the rise time. An advantage of the one-color experiments, however, is the fact that T_0 is easily obtained.) The transients obtained for $CrCO^+$ and Cr^+ (Figure 8a) are strikingly different from the others. In addition to the very short rise times indicating fast formation the $CrCO^+$ signal decays very fast to a rather high constant level, whereas the Cr^+ transient remains at constant maximum intensity, which is of course expected as further fragmentation ultimately leads to the bare metal.

Let us first discuss dynamics B: After the first step of the common model for photofragmentation of $Cr(CO)_6$,[36] i.e., rapid formation of electronically excited $Cr(CO)_5$ (C_{4v}) after pumping into the $^1T_{1u}$ MLCT state, the probe beam should be able to ionize nascent electronically excited $Cr(CO)_5$. The electronic energy of this species according to experiment is 16 000−20 000 cm^{-1},[4] which means that depending on the amount of kinetic energy withdrawn by the departing CO ligand, the nascent fragment possesses at least that amount of energy. The energy necessary to ionize $Cr(CO)_5$ (see Figure 6) can be calculated from the data of Fletcher and Rosenfeld[66] (bond dissociation energy of the neutral parent) and of Qi et al.[39] (bond dissociation energy of the parent ion) and amounts to 62 000 cm^{-1}. Two-photon ionization by the 280 nm probe beam leads to an excess energy of at least 29 500 cm^{-1} for $Cr(CO)_5^+$, which is sufficient to break up to three Cr−CO bonds.[39] Thus the transient peaks observed for the fragments down to $Cr(CO)_2^+$ may arise from the same neutral precursor $Cr(CO)_5$ when considering dynamics B. This could explain why we observe similar behavior for the corresponding transients shown in Figure 7, i.e., a fast pulse width limited rise and decay. From short time scans measured for $Cr(CO)^+_{n=6,3,2}$ not shown here, we observe that the maxima of the peaks are consistently shifted in time with respect to each other by about 20 fs, the $Cr(CO)_6^+$ peak showing the earliest and the $Cr(CO)_2^+$ peak the latest maximum. Due to the noise level, we cannot give an exact number for the peak separation. Additional experiments are in progress. The separation may tentatively be assigned to fast structural changes of the primary photofragment (square pyramid toward trigonal bipyramid in the ^1E state[8,9,36]), leading to different fragmentation yields in the ion channel. To explain the fast decay of the transients shown in Figure 7 and the occurrence of Cr^+ and $CrCO^+$ within dynamics B, we propose further fast fragmentation of the initial neutral $Cr(CO)_5$ down to some fragment possessing enough excess energy that upon probe ionization fragmentation to $CrCO^+$ and Cr^+ can occur. According to the common model of photofragmentation, the fragment is most likely $Cr(CO)_4$. Peifer, Garvey, and DeLeon argued against ultrafast formation of $Cr(CO)_4$ based on time-resolved experiments on the nanosecond time scale.[37] The reason was absence of LIF signal of Cr at early delay times, which they attributed to arising from the $Cr(CO)_4$ intermediate. However, it may well be that the fragmentation steps leading from $Cr(CO)_4$ to ground-state Cr metal occur on a slow time scale, inhibiting observation of the Cr LIF signal at early times.

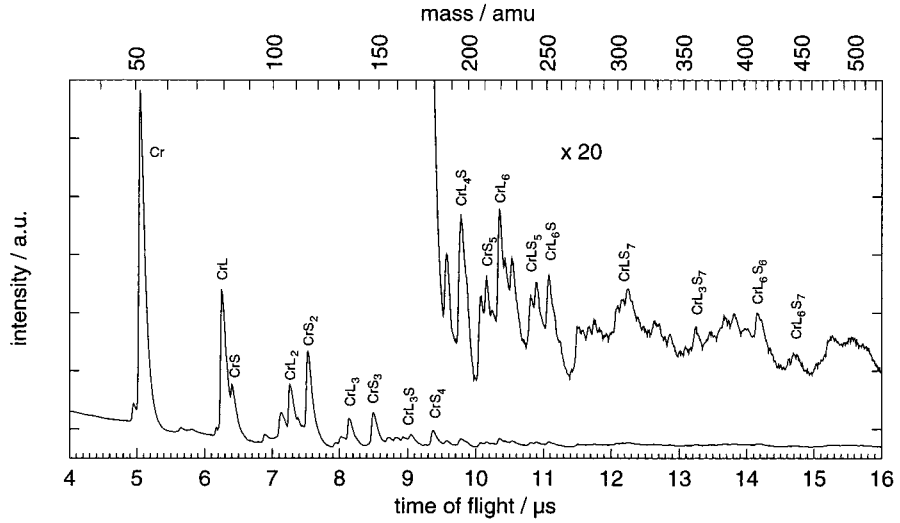

Figure 9. Averaged femtosecond mass spectrum obtained from an expansion of $Cr(CO)_6 \cdot (CH_3OH)_n$ heteroclusters (L = CO, S = CH_3OH).

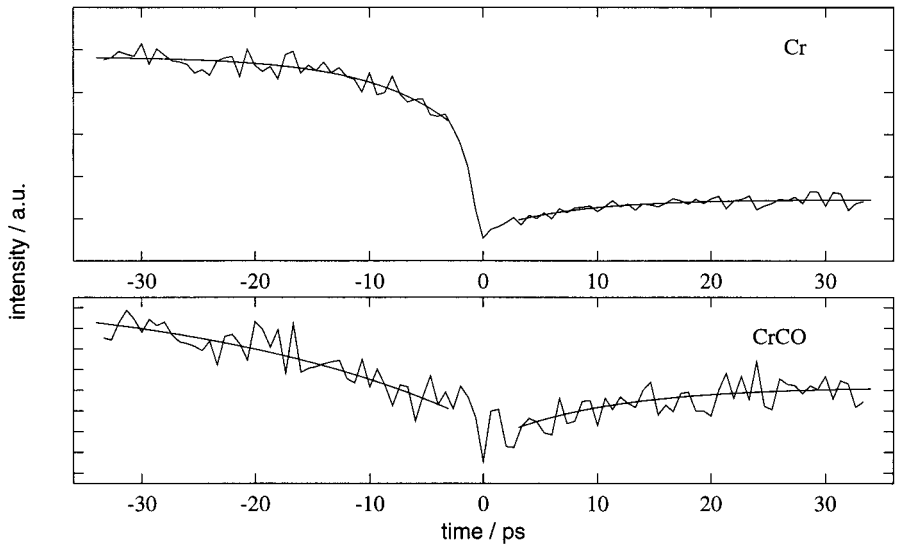

Figure 10. Transients of Cr and CrCO ions obtained from the cluster expansion (weak transients are shown for positive delay times; strong transients are shown for negative delay times). Fits to a single-exponential rise are shown ($\tau_{Cr,strong} = 7.5$ ps, $\tau_{Cr,weak} = 7$ ps, $\tau_{CrCO,weak} = 10$ ps, $\tau_{CrCO,strong} = 24$ ps).

To explain dynamics A, absorption of an additional photon has to take place. As the parent $Cr(CO)_6$ will already be ionized after absorption of an additional photon, nascent $Cr(CO)_5$ (^1E) may be a suitable candidate to start with. Explosive loss of CO ligands may then lead to electronically excited $Cr(CO)_3$, which upon ionization leads to the observed fragment ions not decaying down to zero intensity, i.e. $Cr(CO)_{n=0-3}$. Our findings are qualitatively in line with those of Gerber and co-workers,[69] who considered the photofragmentation of $Fe(CO)_5$. They also observed no detectable rise time and transient peaks for all fragments down to $Fe(CO)_2^+$, a fast rise of 110 fs for $FeCO^+$ which decays within 230 fs to a constant level and a rise of Fe^+ of 260 fs. Their results were interpreted in terms of a concerted, i.e. explosive, ligand loss.

3.2. Dynamics of $Cr(CO)_6 \cdot (CH_3OH)_n$. The mass spectrum of the cluster ions obtained with fs pulses centered at 280 nm is shown in Figure 9. The spectrum is dominated by the bare Cr ion and solvated Cr^+ as well as naked coordinatively unsaturated carbonyl ions. Solvated coordinatively unsaturated carbonyls $Cr(CO)_m^+ \cdot (CH_3OH)_n$ are also present. Their intensities are biased toward lower *m*. The bare parent signal of $Cr(CO)_6^+$ is very small and so are those of the corresponding solvated parent ions. In contrast to the fs mass spectrum obtained from pure $Cr(CO)_6$, solvated $Cr(CO)_4^+$ can be observed after several picoseconds. This hints to the possibility of removing excess energy in either the neutral or the ionic manifold by evaporating solvent molecules rather than by decarbonylation alone. Due to our present (amplifier-limited) mass resolution, we are not able to assign all the peaks at higher masses unambiguously. They will be analyzed in detail in a forthcoming contribution. The dynamics of some of the major mass peaks shown in Figure 9 will now be discussed. Figure 10 shows transients obtained for the naked Cr and CrCO ions, and transients for solvated Cr ions (Cr^+S_2 and Cr^+S_3) are shown in Figure 11. Some transients (weak transients) were taken with pump pulses that were hardly able to ionize the clusters, whereas the probe pulse was strong enough to yield cluster ions by itself. Reversing the order of pump and probe, i.e., allowing for negative delay times, we obtained transients (strong transients) that (apart from signal strength) show behavior different from that of the weak transients. They show an instantaneous rise similar to what was found for the pure $Cr(CO)_6$ transients and assigned to dynamics A above. In addition cluster specific dynamics on the picosecond time scale is readily observed. For

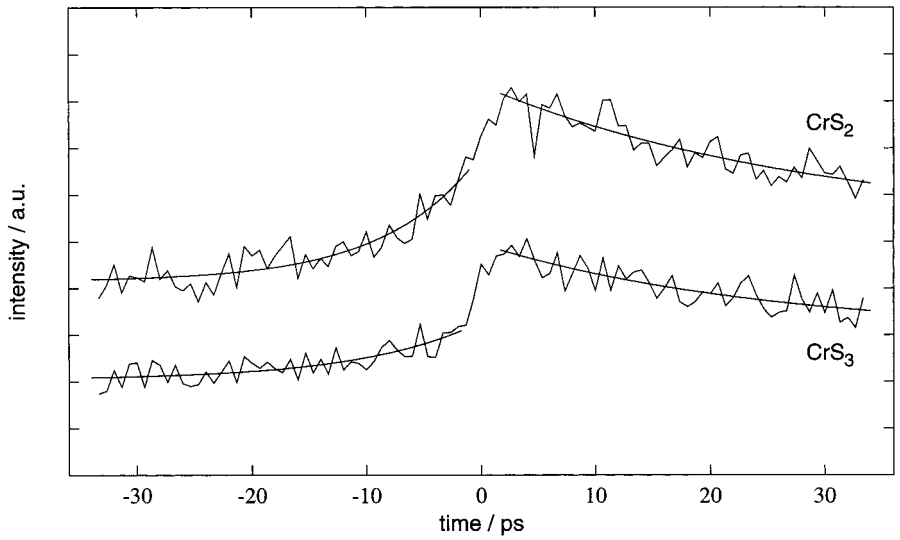

Figure 11. Transients of CrS_2 and CrS_3 ions obtained from the cluster expansion (S = CH_3OH, weak transients are shown for positive delay times; strong transients are shown for negative delay times). The transients are slightly offset with respect to each other. Fits to a single-exponential decay are shown ($\tau_{CrS_2,strong}$ = 8 ps, $\tau_{CrS_2,weak}$ = 30 ps, $\tau_{CrS_2,strong}$ = 10 ps, $\tau_{CrS_2,weak}$ = 25 ps).

Cr^+ the weak transient shows almost no very fast rise. Fitting the long time tail by a single-exponential rise yields a rise time of 7 ps. Picosecond dynamics is also observed for the solvated Cr^+ transients. However, in contrast to the bare Cr^+ transient, the solvated ones after a fast rise show a decay on the picosecond time scale. The solvated photofragments lose solvent molecules by evaporation, yielding less solvated ones and Cr^+. The initial fast rise of the transients is essentially identical to the behavior observed for the pure carbonyls, which we interpreted in terms of fragmentation in the neutral manifold (dynamics B, vide supra). The long time behavior on the ps time scale can simply be interpreted as excess energy release of the coordinatively unsaturated fragments by evaporation of solvent molecules. Such an evaporation can lead to cooling of the initially hot photofragments, which means that we are able to trap higher carbonyls than in the case of isolated $Cr(CO)_6$ decarbonylation, which is clearly reflected in the mass spectrum.

The weak transients of $CrS_{n=2,3}$ show a fast rise followed by a slow decay. The fast rise can be explained as being due to dynamics B occurring within the clusters. Single-exponential fits of the decaying part of the solvated transients shown in Figure 11 yield decay times between 25 and 30 ps. The transients do not reach an asymptotic level in the time range covered by our experiments; additional studies on a longer time scale are in progress. The picosecond rise time of the bare Cr ion transient (7 ps) is shorter than the decay time of the solvated Cr ions. It can thus be concluded that not all solvated Cr atoms decay down to the bare metal. The bare metal ion signal may then arise from two sources, fast decarbonylation of unsolvated $Cr(CO)_6$ according to dynamics B and evaporative solvent loss from hot solvated Cr atoms, presumably formed in small clusters. Due to excess energy loss by evaporation of solvent molecules from higher solvated clusters, the solvated Cr ions are stabilized. The same appears to be true for the coordinatively unsaturated species. The transients of $CrCO^+$ (shown in Figure 10), $Cr(CO)_2^+$, and $Cr(CO)_3^+$ (both very noisy) were measured and showed a significant rise on the picosecond time scale, not reaching an asymptotic level after 30 ps, i.e. rising significantly more slowly than the Cr^+ transient. The fast decay observed in the pure $Cr(CO)_6$ experiments is not observed here; the signal rises slowly instead. This points to a stabilization of the coordinatively unsaturated carbonyls on the picosecond time scale by evaporative loss of solvent molecules withdrawing excess energy. Presently we cannot give an estimate of the cluster size distribution initially excited since solvent loss will occur in both the neutral and the probed ion. However, future experiments will be directed toward investigating larger clusters with the ultimate goal of finding the critical size at which the outgoing CO ligands are trapped in the solvent environment.

The strong solvated Cr^+ transients, on the other hand, show in addition to the pronounced instantaneous rise an immediate first decay followed by a slower decay resembling that of the weak transients. The additional fast decay may be interpreted in a simple classical way assuming dynamics A. As the highly excited primary photofragment $Cr(CO)_5$ loses several CO ligands simultaneously, solvent molecules will be pushed away rapidly by the outgoing ligands. After the first rapid loss of solvent molecules further evaporation on a longer time scale may occur. It should be noted that at least part of the slow decay observed in the strong transients may be due to admixture of weak transient dynamics. However, fitting the slow decay part of the strong transients yields lifetimes (between 8 and 10 ps) that differ from those of the weak transients (Figure 11).

4. Conclusions

In this contribution we reported on our first results of investigating the photodissociation dynamics of transition metal carbonyls and their solvent heteroclusters. The data accumulated for $Cr(CO)_6$ so far can be rationalized in terms of two dynamical channels for decarbonylation, a sequential channel (dynamics B) where excited state (^1E) $Cr(CO)_5$ is the primary photofragment giving rise to very short lived transient ion peaks in the mass spectrum, which further undergoes femtosecond fragmentation into lower coordinated carbonyls, presumably $Cr(CO)_4$. The second channel (dynamics A) observed for intense pump pulses can tentatively be explained as being due to explosive loss of several CO ligands from $Cr(CO)_5$ after absorption of an additional photon from the ^1E state. Experimental hints to the existence of two different fragmentation channels were provided by both the pure $Cr(CO)_6$ and the cluster experiments. For the transients obtained from pure $Cr(CO)_6$ we observed an initial almost simultaneous rise of all fragments studied in addition to a slower rise (still on the sub-100 fs time scale). Furthermore, two different kinds of coordinatively unsaturated photoproducts, $Cr(CO)_2^+$ and

$Cr(CO)_3^+$, could be observed, a species with fast decaying intensity and a species with constant intensity in time. Some further evidence was provided by the solvent heteroclusters. The solvated Cr^+ ions showed different picosecond evaporation dynamics depending on pump pulse intensity, an initial fast loss of solvent molecules in addition to a slower one for intense pump pulses, whereas reduced pump intensity led to observation of only slow evaporation.

For the clusters we find that the essentially pulse width limited femtosecond decarbonylation is significantly faster than evaporation of solvent molecules which occurs on the picosecond time scale. Several solvated fragments and coordinatively unsaturated carbonyls are stabilized by evaporation.

The interpretation of our results given here explains our findings, however, it is still tentative and must be tested by further experiments. Measurements at different wavelengths for both pump and probe pulses have to be performed to check the dependence of the dynamics on the initially excited electronic state and the excess energy delivered into the ion channel. Experiments at different laser intensities will provide information on the importance of the two proposed decarbonylation channels. Investigating the dynamics of additional cluster species and extending the work toward higher solvated clusters will allow us to understand the transition from the isolated single molecule dynamics to that in condensed phase. Research in this direction is currently underway in our laboratory on both the femtosecond and picosecond time scale.

Acknowledgment. Financial support by the Deutsche Forschungsgemeinschaft (Grant Gu 280/3) via the Schwerpunktprogramm "Molekulare Cluster" is gratefully acknowledged. M.S.D. wishes to thank the Fonds der Chemischen Industrie for a graduate fellowship. We also thank Prof. G. Hohlneicher for continuous support.

Note Added in Proof. From experiments on a longer time scale (up to 350 ps) we obtained at least two different evaporation time scales for the solvent heteroclusters (weak transients). The multiexponential rise times found for the Cr^+ transient are from sub-10 ps up to more than 100 ps. Publication of these new results from our laboratory is in preparation.

References and Notes

(1) Andrews, D. L. *Laser Chemistry*; Springer: Berlin, 1986.
(2) Yamamoto, A. *Organotransition Metal Chemistry. Fundamental Concepts and Applications*; Wiley: New York, 1986.
(3) Burdett, J. K.; Perutz, R. N.; Poliakoff, M.; Turner, J. J. *J. Chem. Soc., Chem. Commun.* **1975**, *157*.
(4) Perutz, R. N.; Turner, J. J. *J. Am. Chem. Soc.* **1975**, *97*, 4791.
(5) Perutz, R. N.; Turner, J. J. *J. Am. Chem. Soc.* **1975**, *97*, 4800.
(6) Perutz, R. N.; Turner, J. J. *Inorg. Chem.* **1975**, *14*, 262.
(7) Burdett, J. K.; Graham, M. A.; Perutz, R. N.; Poliakoff, M.; Rest, A. J.; Turner, J. J.; Turner, R. F. *J. Am. Chem. Soc.* **1975**, *97*, 4805.
(8) Burdett, J. K.; Grzybowski, J. M.; Perutz, R. N.; Poliakoff, M.; Turner, J. J.; Turner, R. F. *Inorg. Chem.* **1978**, *17*, 147.
(9) Turner, J. J.; Burdett, J. K.; Perutz, R. N.; Poliakoff, M. *Pure Appl. Chem.* **1977**, *49*, 271.
(10) Kelly, J. M.; Hermann, H.; Koerner von Gustorf, E. *J. Chem. Soc., Chem. Commun.* **1973**, *105*.
(11) Kelly, J. M.; Bent, D. V.; Hermann, H.; Schulte-Frohlinde, D.; Koerner von Gustorf, E. *J. Organomet. Chem.* **1974**, *69*, 259.
(12) Welch, J. A.; Peters, K. S.; Vaida, V. *J. Phys. Chem.* **1982**, *86*, 1941.
(13) Simon, J. D.; Peters, K. S. *Chem. Phys. Lett.* **1983**, *98*, 53.
(14) Simon, J. D.; Xie, X. *J. Phys. Chem.* **1986**, *90*, 6751.
(15) Simon, J. D.; Xie, X. *J. Phys. Chem.* **1987**, *91*, 5538.
(16) Wang, L.; Zhu, X.; Spears, K. G. *J. Am. Chem. Soc.* **1988**, *110*, 8695.
(17) Wang, L.; Zhu, X.; Spears, K. G. *J. Phys. Chem.* **1989**, *93*, 2.
(18) Lee, M.; Harris, C. B. *J. Am. Chem. Soc.* **1989**, *111*, 8963.
(19) Joly, A. G.; Nelson, K. A. *J. Phys. Chem.* **1989**, *93*, 2876.
(20) Joly, A. G.; Nelson, K. A. *Chem. Phys.* **1991**, *152*, 69.
(21) King, J. C.; Zhang, J. Z.; Schwartz, B. J.; Harris, C. B. *J. Chem. Phys.* **1993**, *99*, 7595.
(22) Dougherty, T. P.; Heilweil, E. J. *Chem. Phys. Lett.* **1994**, *227*, 19.
(23) Lian, L.; Bromberg, S. E.; Asplund, M. L.; Yang, H.; Harris, C. B. *J. Phys. Chem.* **1996**, *100*, 11994.
(24) Nathanson, G.; Gitlin, B.; Rosan, A. M.; Yardley, J. T. *J. Chem. Phys.* **1981**, *74*, 361.
(25) Yardley, J. T.; Gitlin, B.; Nathanson, G.; Rosan, A. M. *J. Chem. Phys.* **1981**, *74*, 370.
(26) Tumas, W.; Gitlin, B.; Rosan, A. M.; Yardley, J. T. *J. Am. Chem. Soc.* **1982**, *104*, 55.
(27) Fletcher, T. R.; Rosenfeld, R. N. *J. Am. Chem. Soc.* **1985**, *107*, 2203.
(28) Tyndall, G. W.; Jackson, R. L. *J. Chem. Phys.* **1989**, *91*, 2881.
(29) Breckenridge, W. H.; Stewart, G. M. *J. Am. Chem. Soc.* **1986**, *108*, 364.
(30) Holland, J. P.; Rosenfeld, R. N. *J. Chem. Phys.* **1988**, *89*, 7217.
(31) Seder, T. A.; Church, S. P.; Weitz, E. *J. Am. Chem. Soc.* **1986**, *108*, 4721.
(32) Weitz, E. *J. Phys. Chem.* **1987**, *91*, 3945.
(33) Wells, J. R.; Weitz, E. *J. Am. Chem. Soc.* **1992**, *114*, 2783.
(34) Weitz, E. *J. Phys. Chem.* **1994**, *98*, 11256.
(35) Mikami, N.; Ohki, R.; Kido, H. *Chem. Phys.* **1988**, *127*, 161.
(36) Venkataraman, B.; Hou, H.; Zhang, Z.; Chen, S.; Bandukwalla, G.; Vernon, M. *J. Chem. Phys.* **1990**, *92*, 5338.
(37) Peifer, W. R.; Garvey, J. F.; DeLeon, R. L. *J. Phys. Chem.* **1992**, *96*, 6523.
(38) Qi, F.; Yang, X.; Yang, S.; Liu, F.; Sheng, L.; Gao, H.; Zhang, Y.; Yu, S. *J. Chem. Phys.* **1997**, *106*, 9474.
(39) Qi, F.; Yang, X.; Yang, S.; Gao, H.; Sheng, L.; Zhang, Y.; Yu, S. *J. Chem. Phys.* **1997**, *107*, 4911.
(40) Qi, F.; Yang, S.; Sheng, L.; Ye, W.; Gao, H.; Zhang, Y.; Yu, S. *J. Phys. Chem.* **1997**, *101*, 7194.
(41) Duncan, M. A.; Dietz, T. G.; Smalley, R. E. *Chem. Phys.* **1979**, *44*, 415.
(42) Whetten, R. L.; Fu, K.-J.; Grant, E. R. *J. Chem. Phys.* **1983**, *79*, 4899.
(43) Gerrity, D. P.; Rothberg, L. J.; Vaida, V. *J. Phys. Chem.* **1983**, *87*, 2222.
(44) Tyndall, G. W.; Jackson, R. L. *J. Am. Chem. Soc.* **1987**, *109*, 582.
(45) Tyndall, G. W.; Jackson, R. L. *J. Chem. Phys.* **1988**, *89*, 1364.
(46) Tyndall, G. W.; Larson, C. E.; Jackson, R. L. *J. Phys. Chem.* **1989**, *93*, 5508.
(47) Jackson, R. L. *Acc. Chem. Res.* **1992**, *25*, 581.
(48) Kim, S. K.; Pederson, S.; Zewail, A. H. *Chem. Phys. Lett.* **1994**, *233*, 500.
(49) Bañares, L.; Baumert, T.; Bergt, M.; Kiefer, B.; Gerber, G. *Chem. Phys. Lett.* **1997**, *267*, 141.
(50) Peifer, W. R.; Garvey, J. F. *J. Chem. Phys.* **1991**, *94*, 4821.
(51) Peifer, W. R.; Garvey, J. F. *J. Phys. Chem.* **1991**, *95*, 1177.
(52) Lyktey, M. Y. M.; Xia, P.; Garvey, J. F. *Chem. Phys. Lett.* **1995**, *238*, 54.
(53) Beach, N. A.; Gray, H. B. *J. Am. Chem. Soc.* **1968**, *90*, 5713.
(54) Hay, P. J. *J. Am. Chem. Soc.* **1978**, *100*, 2411.
(55) Li, J.; Schreckenbach, G.; Ziegler, T. *J. Phys. Chem.* **1994**, *98*, 4838.
(56) Barnes, L. A.; Liu, B.; Lindh, R. *J. Chem. Phys.* **1993**, *98*, 3978.
(57) Persson, B. J.; Roos, B. O. *J. Chem. Phys.* **1994**, *101*, 6810.
(58) Pierloot, K.; Tsokos, E.; Vanquickenborne, L. G. *J. Phys. Chem.* **1996**, *100*, 16545.
(59) Pollak, C.; Rosa, A.; Baerends, E. J. *J. Am. Chem. Soc.* **1997**, *119*, 7324.
(60) Greenfield, S. R.; Wasielewski, M. R. *Opt. Lett.* **1995**, *20*, 1394.
(61) Wiley, W. C.; McLaren, I. H. *Rev. Sci. Instrum.* **1955**, *26*, 1150.
(62) Weinkauf, R.; Aicher, P.; Wesley, G.; Grotemeyer, J.; Schlag, E. W. *J. Phys. Chem.* **1994**, *98*, 8381.
(63) Wei, S.; Castleman, A. W., Jr. In *Chemical Reactions in Clusters*; Bernstein, E. R., Ed.; Oxford University Press: New York, 1996; p 197.
(64) Higginson, B. R.; Lloyd, D. R.; Burroughs, P.; Gibson, D. M.; Orchard, A. F. *J. Chem. Soc., Faraday Trans. 2* **1973**, *69*, 1659.
(65) Trushin, S. A.; Fuss, W.; Schmid, W. E.; Kompa, K. L. *The 3rd Conference on Femtochemistry* (August 31−September 4, 1997 Lund, Sweden); Book of Abstracts P. 85; work submitted to special issue of *J. Phys. Chem.* "Femtochemistry-97".
(66) Fletcher, T. R.; Rosenfeld, R. N. *J. Am. Chem. Soc.* **1988**, *110*, 2097.